# Architecture-dependent signal conduction in model networks of endothelial cells

Pierre A. Deymier,[1] Mete Eray,[2] Martin J. Deymier,[3] Keith Runge,[1] James B. Hoying,[4] and Jérome O. Vasseur[5]
[1]*Materials Science and Engineering Department, University of Arizona, Tucson, Arizona 85721, USA*
[2]*Department of Electrical and Computer Engineering, University of Arizona, Tucson, Arizona 85721, USA*
[3]*Department of Biochemistry and Department of Molecular Cell Biology, University of Arizona, Tucson, Arizona 85721, USA*
[4]*Cardiovascular Innovation Institute, School of Medicine, University of Louisville, Louisville, Kentucky 40292, USA*
[5]*EPHONI, IEMN, UMR CNRS 8520, Université de Lille 1, Villeneuve d'Ascq, 59655 Lille, France*
(Received 8 August 2009; revised manuscript received 17 February 2010; published 19 April 2010)

Signal conduction between endothelial cells along the walls of vessels appears to play an important role in circulatory function. A recently developed approach to calculate analytically the spectrum of propagating compositional waves in models of multicellular architectures is extended to study putative signal conduction dynamics across networks of endothelial cells. Here, compositional waves originate from negative feedback loops, such as between $Ca^{2+}$ and inositol triphosphate ($IP_3$) in endothelial cells, and are shaped by their connection topologies. We consider models of networks constituted of a main chain of endothelial cells and multiple side chains. The resulting transmission spectra encode information concerning the position and size of the side branches in the form of gaps. This observation suggests that endothelial cell networks may be able to "communicate" information regarding long-range order in their architecture.

DOI: 10.1103/PhysRevE.81.041915 PACS number(s): 87.18.Mp, 87.18.Fx, 87.18.Hf, 87.17.Pq

## I. INTRODUCTION

A functional microcirculation consists of different microvessel types (generally defined as arterioles, capillaries, and venules) organized into a network comprising an effective perfusion circuit. During embryo development or following an angiogenesis burst during tissue repair in the adult, an immature network must remodel and adapt in order to form an effective new vascular tree. In the embryo, a new vascular plexus forms as the result of vasculogenesis that eventually evolves through a process involving artery-vein specification, vessel revision, and vessel remodeling [1]. During neovascularization following implantation, an immature plexus forms from existing vascular elements that eventually forms a hierarchical vascular tree [2]. In both situations, inflow-outflow paths are necessarily redefined, vessel diameters are expanded or rarefied (structural adaptation), and network architecture is reorganized. Given that these activities are all related to forming a new network, they suggest that coordination of changes within individual vessel elements across the forming network must occur. However, very little is known concerning what, if any, long-range network-wide signal dispersion occurs or if the different types of information inherent in such global information transfer are relevant in the vasculature.

A theoretical analysis of the responses to the many different integrated stimuli leading to structural adaptation of microvessels predicts that an upstream transfer of information from the distal vessels to arterioles and feed arteries is required [3]. While no molecular or cellular mechanism of signal conduction specific to this structural adaptation response or the other aspects of network revision has been identified, other examples of signal propagation within the microvessel network have been described. Stimulation of distal microvessels with adenosine triphosphate (ATP) or acetylcholine leads to the dilation of upstream microvessels [4,5]. These examples of vasoactive-related signal conduction have primarily involved signal propagation along a single contiguous line of vessel elements along a relatively modest distance. The mechanisms of signal conduction in these situations are not fully defined. However, intracellular $Ca^{2+}$ dynamics and gap junction activity are likely to be important [6,7]. Whether or not these vasoactivity-related mechanisms might also be the basis for a network-wide communication scheme is not known. One way to address this is to define the theoretical structure of such a communication system and determine if known conduction processes are capable of functioning in the necessary capacity.

In considering the hypothetical phenomena of network-wide communication, the types of information that could be relevant must combine dynamical and structural complexity. The problem at hand is, therefore, to construct a framework for integrating models of intracellular pathways with nontrivial multicellular architectures including cell-to-cell interactions. The signaling pathways could be described by coupled linear or nonlinear multicomponents reactions. The nontrivial multicellular architectures may be one, two, and three dimensional with topological complexity. Cell-to-cell interactions may include short- and long-range diffusion-driven (involving mass transport) or signal-driven (nondiffusive) coupling.

Therefore, we set out to develop a theoretical model of network-wide distribution of information along a network of endothelial cells. We are exploring a possible mechanism of information transmission through long-range signal conduction along chains and networks of chains of endothelial cells. These wavelike signals originate from (a) negative feedback loops between $Ca^{2+}$ and inositol 1,4,5-triphosphate ($IP_3$) in endothelial cells and (b) cell-to-cell interactions and contain information on the spatial structure of the networks encoded in their wave-number (frequency) spectrum. Recently, $Ca^{2+}$ waves that propagate along the endothelium have been shown to act as long-range signals that contribute to vasodilation of arterioles [6]. Gap junctions between cells can also facilitate the transmission of $Ca^{2+}$ signals between cells to

 

control blood vessel function [7]. There are other examples of multicellular networks such as the folliculate cell network in the pituitary gland that form circuitry in which information is relayed over long distances via $Ca^{2+}$ wave propagation [8]. In this example, $Ca^{2+}$ wave propagation was shown to depend on gap junction signaling. At the level of the individual cell, these signals rely on the intake or release of $Ca^{2+}$ ions from intracellular stores such as the endoplasmic reticulum (ER). The physiological state of the cytoplasm of a cell determines the nature of the dynamics of calcium release and intake [9]. The physiological state may be bistable with two resting states for calcium concentration; low basal and high corresponding to replete ER and empty ER, respectively, and separated by an intermediate unstable threshold concentration. The bistable state may lead to traveling fronts in spatially extended systems. The physiological state may also be that of an excitable cytoplasm and may be considered to be a variant on the bistable state with the possibility of returning to the low basal concentration beyond a high cytosol concentration threshold. Excitable cytoplasm may produce pulse waves in spatially extended systems. Finally, many cells exhibit oscillatory cytoplasm states which may lead to waves with temporal and spatial periodicity.

Within this context, the objective of the present study is to investigate the dependence of long-range compositional signals on cell network architecture in models of endothelial cell networks. This work is based on a recently established linear theory of multicellular networks that enables the determination of architecture-dependent compositional excursions from steady-state values in the form of compositional traveling waves [10]. Starting from an infinite length chain of endothelial cells serving as a backbone, the theory is used to build increasingly more complex networks by grafting side chains of cells onto the backbone. These models of endothelial cell networks show that resonant filtering of propagating compositional waves with specific wavelength (wave number), a nontrivial behavior, emerges as a result of adjoining the finite length segments of cells onto the backbone. For periodic or nearly periodic arrangements of side chains along the backbone, additional filtering arises from scattering by the periodic structure. We show that the complete spectrum of propagating signals contains superposed and separate structural information concerning the spacing between the side branches as well as the length of the side branches.

In Sec. II of this paper, we review in some detail the linear theory of multicellular networks. We pay particular attention to the application of the theory to calcium signals in branched networks of endothelial cells. Signal propagation is analyzed in terms of transmission spectra in the results and discussion section (Sec. III). In that section, we demonstrate that the transmission spectra contain information that relates to the length of the side chains as well as their arrangements along the backbone. Conclusions are drawn in Sec. IV.

## II. MODELS AND METHODS

### A. Reaction-diffusion model of a chain of endothelial cells

Othmer and Scriven, while analyzing the onset of instability at homogeneous steady states of multicellular networks, developed an elegant method that decouples the intracellular biochemical dynamics from the network structure of an underlying reaction-diffusion problem [11,12]. They assumed a mixture of $n$ reactants in each one of the $N$ cells, each attached to one or more other cells to form the desired topology. The small excursions around the steady-state concentration values of cell $\mu$ is represented by the $n\times 1$ vector $\mathbf{x}^{(\mu)}$ which is solution of a linear vector differential equation given by

$$\frac{d\mathbf{x}^{(\mu)}}{dt} = \mathbf{D}\Delta^{(\mu)}\mathbf{x}^{(\mu)} + \mathbf{K}\mathbf{x}^{(\mu)}, \quad \mu = 1, \ldots, N. \tag{1}$$

The first term following the equal sign gives the rates of change due to transfer between directly interacting cells. The rates of change due to intracellular reactions are represented by the second term. The elements $d_{ij}$, $i,j=1,\ldots,n$, of the $n\times n$ transfer matrix $\mathbf{D}$ quantify the effect of reactant $j$ on the transfer of reactant $i$ through the barrier separating adjacent cells. The $n\times n$ Laplacian $\Delta^{(\mu)}\mathbf{x}^{(\mu)}=\mathbf{x}^{(\mu+1)}(t)-2\mathbf{x}^{(\mu)}(t)+\mathbf{x}^{(\mu-1)}(t)$ in Eq. (1) encodes the connection pattern among the cells. We use $\mathbf{C}_\mathbf{x}$ to represent the resulting structural matrix. For instance the structural matrix $\mathbf{C}_\infty$ of an infinite chain of cells [see Fig. 1(a)] has the familiar tridiagonal form

$$\mathbf{C}_\infty = \begin{pmatrix} \ddots & \ddots & \ddots & \ddots & & & & & & \\ \ddots & \ddots & \ddots & \ddots & \ddots & & & & & \\ \cdots & 0 & 1 & -2 & 1 & 0 & \cdots & & & \\ & \cdots & 0 & 1 & -2 & 1 & 0 & \cdots & & \\ & & \cdots & 0 & 1 & -2 & 1 & 0 & \cdots & \\ & & & \cdots & 0 & 1 & -2 & 1 & 0 & \cdots \\ & & & & & \ddots & \ddots & \ddots & \ddots & \ddots \\ & & & & & & \ddots & \ddots & \ddots & \ddots \end{pmatrix}. \tag{2}$$

The three nonzero entries in each row correspond to the coefficients in the discrete approximation of the Laplacian.

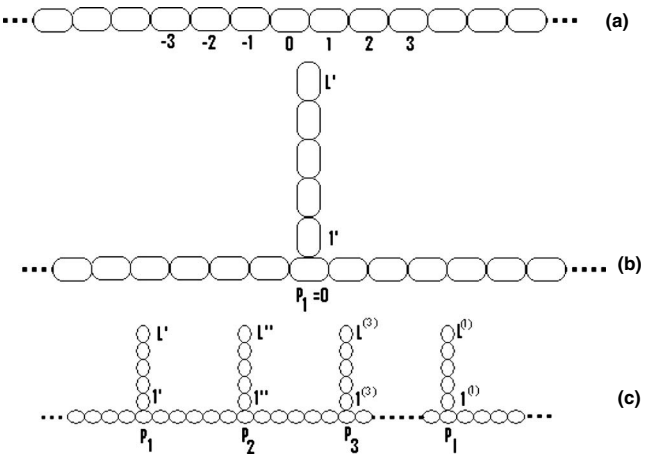


FIG. 1. (a) Multicellular chain forming an infinite backbone for the formation of composite cellular networks by coupling (b) a single side chain of length $L'$ on an infinite backbone and (c) multiple chains along the backbone.

In Eq. (1), the reaction matrix $\mathbf{K}$ represents a linearized intracellular reaction dynamics with the elements, $k_{ij}$, $i,j=1,\ldots,n$, representing the collective effect of reactant $j$ on the reactant $i$. Assuming spatially homogeneous systems, both $\mathbf{D}$ and $\mathbf{K}$ are cell independent. The time progress of concentration excursions in all of the cells are concatenated into a $Nn\times 1$ column vector given by

$$\bar{\mathbf{x}}(t)=\sum_{k=1}^{N}\mathbf{u}_k\otimes e^{(\mathbf{K}+\alpha_k\mathbf{D})t}\mathbf{y}_k^0, \tag{3}$$

with $\otimes$ representing the tensor product. In Eq. (3), $\alpha_k$ and $\mathbf{u}_k$, $k=1,\ldots,N$, are the eigenvalues and eigenvectors of the connectivity matrix, $\mathbf{C}_\mathbf{x}$, respectively. The $n\times 1$ vector $\mathbf{y}_k^0$ is the projection of the initial condition vector $\bar{\mathbf{x}}_0=\bar{\mathbf{x}}(t=0)$ onto a derived set of basis vectors spanning the vector space that includes $\mathbf{x}(t)$.

The intracellular model that we consider here is that of small concentration excursions in the form of small amplitude oscillations surrounding a stable point in the dynamics of a cytoplasm. Our model may also represent low amplitude oscillations in an oscillatory cytoplasm. These oscillatory intracellular behaviors may be considered to result from complex feedback loops. As an example, we treat the case of a two-component negative feedback loop where one compound activates the production of the second which in turn inhibits the first one. Within endothelial cells of arterioles, a calcium based signaling pathway exists that contains a two-component negative feedback loop. This loop occurs between $Ca^{2+}$ and $IP_3$. This inositol phospholipid signaling pathway is started by an extracellular signal molecule that activates a transmembrane G-protein coupled receptor which in turn activates phospholipase C-$\beta$. Phospholipase C-$\beta$ cleaves intracellular membrane bound phospho inositol 4,5-bisphosphate $[PI(4,5)P_2]$ causing the cytoplasmic release of $IP_3$. Cytoplasmic $IP_3$ can bind and open $IP_3$ gated $Ca^{2+}$ channels in the endoplasmic reticulum leading to increased cytoplasmic $Ca^{2+}$ concentration. $IP_3$ concentration is degraded by phosphorylation via $Ca^{2+}$ regulated kinase. The cytoplasmic inositol 1,4,5-triphosphate 3-kinases ($IP_3Ks$) are a group of calcium-regulated inositol polyphosphate kinases that convert $IP_3$ into inositol 1,3,4,5-tetrakisphosphate. This later specie is inactive as a $Ca^{2+}$ release inducer, thus reducing intracellular $Ca^{2+}$ concentration. The overall effect of this signaling cascade is that of a two component ($Ca^{2+}$ and $IP_3$) negative feedback loop. This type of feedback loop has been shown to lead to $Ca^{2+}$ and $IP_3$ oscillations. Of relevance here, the frequency of these oscillations can be controlled by cellular signaling [13]. For the sake of mathematical tractability, the model developed herein assumes intracellular reaction dynamics involving only the two chemical species (i.e., $n=2$): $IP_3$ and $Ca^{2+}$. The model is simplified further by linearization of the reaction dynamic equations. Therefore, for the intracellular dynamics, an activator-inhibitor pair is assumed so that

$$\mathbf{K}=\begin{pmatrix} r' & -r \\ r & r' \end{pmatrix}. \tag{4}$$

We further assume that the active and passive diffusivities are the same for both reactants such that

$$\mathbf{D}=\begin{pmatrix} d' & d \\ d & d' \end{pmatrix}. \tag{5}$$

The constants $d'$, $r'<0$ on the main diagonals are self regulation terms whereas the off-diagonal terms $d>0$, $r<0$ are cross coupling terms. The opposite signs for the off-diagonal elements in $\mathbf{K}$ are sufficient to obtain a self oscillatory behavior for negligible $r'$ [14].

To illustrate the construction of a solution for the composition along an infinite chain, we write the eigenvalues and eigenvectors corresponding to the operator matrix of Eq. (2) [15]:

$$\alpha_k=-4\sin^2\left(\frac{ka_0}{2}\right),$$

$$\mathbf{u}_k=(\cdots\quad e^{-ika_0}\quad 1\quad e^{ika_0}\quad\cdots)^T, \tag{6}$$

where $k$ is the propagation constant and $a_0$ is the lattice constant. $\mathbf{u}_k$ is a discrete complex sinusoidal function with wave number $k$. $k$ is a measure of the spatial variation in the eigenvectors. The eigenvectors of Eq. (6) correspond to propagating waves, periodic function in $ka_0$ defined over the interval $[-\pi,\pi]$. By symmetry we limit this interval to the positive half, namely, $[0,\pi]$. These eigenvectors are isomorphic to vibrational waves in a one-dimensional harmonic crystal defined on the positive half of the first Brillouin zone.

Notice that each eigenvector is of infinite length and its $m$th element $u_{k,m}$ represents the $m$th cell in the chain, where $m$ is an integer. We also use initial profiles of spatial exponential variations of wave vector $k_0$ for both reactants in cell $m$. With an arbitrary phase difference of $-\pi\leq\theta\leq\pi$, the initial condition for cell $m$ is chosen to be

$$\mathbf{x}_0^{(m)}=\begin{pmatrix} e^{ik_0a_0m} \\ e^{i(k_0a_0m+\theta)} \end{pmatrix}. \tag{7}$$

After a significant amount of algebra, assuming $d\sim 0$ and taking $\theta=-\pi/2$, the composition vector of Eq. (3) is obtained in the form

$$\mathbf{x}^{(m)}(t)=\begin{pmatrix} e^{(r'+\alpha_{k_0}d')t}e^{i(k_0a_0m+rt)} \\ -ie^{(r'+\alpha_{k_0}d')t}e^{i(k_0a_0m-rt)} \end{pmatrix}. \tag{8}$$

The profile for the first component has a backward traveling-wave component $e^{i(k_0a_0m+rt)}$ and the second, a forward traveling-wave component $e^{i(k_0a_0m-rt)}$. Both profiles also share a common attenuation term $e^{(r'+\alpha_{k_0}d')t}$. The initial $-\pi/2$ phase difference is preserved and both waves travel at a constant speed, $v=r/k_0$. The leading attenuation term disappears when $r'+\alpha_{k_0}d'=0$. This later condition implies that the cells are able to regulate $r'$ for a given wave vector. Moreover, control of the frequency of the traveling-wave term in Eq. (8) requires that endothelial cells are able to regulate $r$. Frequency of the $Ca^{2+}$ and $IP_3$ oscillations has been shown to be controlled in endothelial cells by stimulus concentration [13].

### B. Network of endothelial cells composed of a backbone with side chains

To integrate biological organization from cellular level to complex network architecture, we use the interface response theory (IRT). IRT augments Scriven-Othmer's method by solving for the eigenvalues and eigenvectors of nontrivial connectivity matrices [15]. A uniform chain of infinitely many cells is used as a reference system and subsequently denoted the bulk system. The Green's function $\mathbf{G}_0$ of the bulk system is the inverse of an operator $\mathrm{H}_0$ (here characterized by the connectivity matrix, $C_\infty$) that represents the interactions among cell sites along the chain. The element $G_0(n,n')$ of the bulk Green's function denotes the effect observed at site $n$ in response to a perturbation applied at site $n'$. Our objective is therefore to determine the Green's function $g$ of nonuniform composite networks of cells. The Green's function of a composite network, $g$, is the inverse of the connectivity matrix, $C_x$. This later matrix has lost the tridiagonality of the bulk chain and its inversion is therefore not trivial. IRT was developed to address this issue. A review paper [16] and references therein list some of the application areas of IRT to condensed matter physics with numerous examples from the literature. The integration of Othmer and Scriven's approach and the IRT to the development of a linear theory of biological networks and architecture was recently reported [10].

IRT is used to calculate the eigenvalues and eigenvectors of structural matrices describing multicellular networks from homogeneous infinite bulk structure through series of coupling operations. We illustrate the IRT for the construction of nontrivial architectures by first coupling a single finite-length chain of cells onto an infinite backbone chain of cells [Figs. 1(b)] and multiple side-chains on the same backbone [Fig. 1(c)]. We use $M$ to denote the set of sites within the interface domain of the nontrivial architectures. For a single side chain, $M$ is composed of the sites $\{p_1,1'\}$ where $p_1$ is also taken as the origin along the backbone. $D$ denotes the space of the composite architecture, that is, any site $n$ along the backbone or any site $j'$ along the side chain. In the case of the network composed of multiple side branches, $M$ includes the sites $\{p_1,1',p_2,1'',p_3,1^{(3)},\ldots,p_l,1^{(l)}\}$. Again the space $D$ is that of any site along the backbone or the side branches. The eigenvectors of a composite system depend on those of the bulk system as given by [17]

$$\mathbf{u}(D) = \mathbf{U}(D) - \mathbf{U}(M)^T\boldsymbol{\Delta}^{-1}(M,M)\mathbf{A}(M,D), \tag{9}$$

where $\mathbf{U}(D)$ is an eigenvector of the collection of individual bulk systems prior to the coupling operation. $\mathbf{U}(M)$ is the same eigenvector but limited to the interface domain $M$. $\mathbf{A}$ is defined as the interface response operator with the first argument giving the sites of the response in $M$ and the second, the site of the action in $D$ that leads to the response. The matrix $\boldsymbol{\Delta}(M,M)$ is defined as $\mathbf{I}_M+\mathbf{A}(M,M)$, where $\mathbf{I}_M$ is an identity matrix with the dimensions of the set $M$. $\mathbf{A}(M,D)$ can be written in terms of a perturbing operator (such as a coupling operator), $\mathbf{V_I}(M,M)$, applied to the Green's function between points in $M$ and $D$ as given by

$$\mathbf{A}(M,D) = \mathbf{V_I}(M,M)\mathbf{G}(M,D). \tag{10}$$

Notice that $\mathbf{G}(M,D)$ is the Green's function of a reference composite system prior to the coupling, i.e., an infinite chain and uncoupled finite chains of cells. It is constructed from the Green's functions of the homogeneous constitutive media limited to the geometrical domains of the finite constitutive blocks used to build the final architecture.

We review briefly the method in the case of the multicellular network composed of an infinite chain [Fig. 1(b)] with a single finite side chain. For the cellular system given in Fig. 1(b), the spaces $D$ and $M$ are defined as $D=\{D_1=\{-\infty,\ldots,-1,0,1,\ldots,\infty\}\}\cup\{D_2=\{1',2',\ldots,L'\}\}$ and $M=\{0,1'\}$. The coupling operator is a $2\times2$ matrix, $\mathbf{V_I}(M,M)$, given by

$$\mathbf{V_I}(M,M) = \begin{pmatrix} -1 & 1 \\ 1 & -1 \end{pmatrix}. \tag{11}$$

In this matrix, the first and second columns or rows correspond to the cell at location $p1=0$ of the infinite chain and the cell $1'$ at the tip of the side chain, respectively. Depending on its arguments, $\mathbf{G}(M,D)$ can take one of four possible forms;

$$\mathbf{G}(m\in M, n\in D) = \begin{cases} \mathbf{G_0}(m,n), & \text{if } m=0 \text{ and } n\in D_1 \\ 0, & \text{if } m=1' \text{ and } n\in D_1 \\ \mathbf{g_s}(m,n), & \text{if } m=1 \text{ and } n\in D_2 \\ 0, & \text{if } m=0 \text{ and } n\in D_2, \end{cases} \tag{12}$$

where $\mathbf{G_0}$ is the Green's function of the infinite chain and $\mathbf{g_s}$ is that of the side chain. $\mathbf{G_0}$ was previously given as [18]

$$\mathbf{G_0}(m,n) = \frac{t^{|m-n|+1}}{t^2-1}, \tag{13}$$

where $t=e^{ika_0}$. $\mathbf{g_s}$ was derived as [19]

$$\mathbf{g}_s(m,n) = \frac{t^{|m-n|+1}+t^{(m+n)}}{t^2-1} + \frac{t^{2L'+1}}{(t^2-1)(1-t^{2L'})} \times (t^{(1-m-n)}+t^{(n-m)}+t^{(m-n)}+t^{(m+n-1)}), \tag{14}$$

where $L'$ is the length of the side branch. The boundary conditions at the ends of the finite segment are reflective.

For the multicellular network composed of multiple chains [Fig. 1(c)], we define the spaces $D$ and $M$ as

$$D=\{-\infty,\ldots,-1,0,1,\ldots,\infty\}\cup\{\{1',2',\ldots,L'\}, \{1'',2'',\ldots,L''\},\{1^{(3)},2^{(3)},\ldots,L^{(3)}\},\ldots,\{1^{(l)},2^{(l)},\ldots,L^{(l)}\}\}$$

and $M=\{p_1=0,1',p_2,1'',p_3,1^{(3)},\ldots,p_l,1^{(l)}\}$. In this case, the coupling operator is a $2N_c\times2N_c$ matrix (where $N_c$ is the number of side chains) which form is given by

$$V_I(M,M) = \begin{pmatrix} -1 & 1 & 0 & 0 & \cdots & 0 & 0 \\ 1 & -1 & 0 & 0 & \cdots & 0 & \vdots \\ 0 & 0 & -1 & 1 & \cdots & 0 & 0 \\ 0 & 0 & 1 & -1 & \cdots & 0 & 0 \\ \vdots & \vdots & \vdots & \vdots & \cdots & \vdots & \vdots \\ 0 & 0 & 0 & 0 & 0 & -1 & 1 \\ 0 & 0 & 0 & 0 & 0 & 1 & -1 \end{pmatrix}. \tag{15}$$

To calculate $\Delta(M,M)=I(M,M)+V_I(M,M)G(M,M)$, one needs the Green's function of the reference system, $G(M,M)$, which takes the form for our model of a network:

$$G(M,M) = \begin{pmatrix} G_0(p_1p_1) & 0 & G_0(p_1p_2) & 0 & G_0(p_1p_3) & 0 & \cdots & G_0(p_1p_l) & 0 \\ 0 & g_s(1'1') & 0 & 0 & 0 & 0 & \cdots & 0 & 0 \\ G_0(p_2p_1) & 0 & G_0(p_2p_2) & 0 & G_0(p_2p_3) & 0 & \cdots & G_0(p_2p_l) & 0 \\ 0 & 0 & 0 & g_s(1''1'') & 0 & 0 & \cdots & 0 & 0 \\ G_0(p_3p_1) & 0 & G_0(p_3p_2) & 0 & G_0(p_3p_3) & 0 & \cdots & G_0(p_3p_l) & 0 \\ 0 & 0 & 0 & 0 & 0 & g_s(1^{(3)}1^{(3)}) & \cdots & 0 & 0 \\ \vdots & \vdots & \vdots & \vdots & \vdots & \vdots & \vdots & \vdots & \vdots \\ G_0(p_lp_1) & 0 & G_0(p_lp_2) & 0 & G_0(p_lp_3) & 0 & \cdots & G_0(p_lp_l) & 0 \\ 0 & 0 & 0 & 0 & 0 & 0 & \cdots & 0 & g_s(1^{(l)}1^{(l)}) \end{pmatrix}. \tag{16}$$

In this matrix the odd entries (row or column) correspond to locations along the backbone in $M$ and the even entries correspond to the position of the first cell of the side branches (also in the space $M$). From Eqs. (13) and (14), the elements of this matrix are therefore

$$G_0(p_i,p_j) = \frac{t^{|p_i-p_j|+1}}{t^2-1} \quad \text{and}$$

$$g_s(1^{(i)},1^{(i)}) = \frac{t+t^{L_i}}{(t-1)(1-t^{2L_i})}. \tag{17}$$

We chose the reference eigenvector $U(D)$ to correspond to a plane-wave propagating along the backbone only such that $U(D)=\{t^n,0\}$. This vector is nonzero for any site, $n$, along the infinite chain, and zero in the finite side chains. The eigenvectors of the network structure along the backbone take the form

$$u_k^n = e^{ika_0n} - [1-\hat{T}(ik)]e^{-ika_0n} \quad \text{if } n \le p_1,$$

$$u_k^n = \hat{T}(ik)e^{ika_0n} \quad \text{if } n > p_l,$$

$$u_k^n = e^{ika_0n} - [1-\hat{T}_A(ik)]e^{-ika_0n} - \hat{T}_B(ik)e^{ika_0n} \quad \text{if } p_i < n \le p_{i+1}, \tag{18a}$$

where

$$\hat{T}(ik) = 1 - U(M)\Delta^{-1}(M,M)\frac{1}{(e^{ika_0})^2-1} \times(-e^{ika_0(1-p_1)} \; e^{ika_0(1-p_1)} \; \ldots \; -e^{ika_0(1-p_l)} \; e^{ika_0(1-p_l)}), \tag{18b}$$

$$\hat{T}_A(ik) = 1 - U(M)\Delta^{-1}(M,M)\frac{1}{(e^{ika_0})^2-1} \times(-e^{ika_0(1-p_1)} \; e^{ika_0(1-p_1)} \; \cdots \; -e^{ika_0(1-p_i)} \; e^{ika_0(1-p_i)} \; 0 \cdots), \tag{18c}$$

$$\hat{T}_B(ik) = U(M)\Delta^{-1}(M,M)\frac{1}{(e^{ika_0})^2-1} \times(0 \cdots 0 - e^{ika_0(1+p_{i+1})} \; e^{ika_0(1+p_{+1i})} \cdots - e^{ika_0(1+p_l)}). \tag{18d}$$

To obtain the composition excursions along the backbone, we employ the same initial condition as that of the infinite chain given by Eq. (7) with $\theta=\pi/2$. Combining Eqs. (3) and (7), and (18) and after numerous algebraic steps and assuming that we neglect self promotion/degradation $r' \sim 0$ and diffusion $d' \sim 0$, the compositional variations along a backbone of a branched system at some cell $m$ beyond the branched region of the backbone are given in compact form by

$$x^{(m)}(t) = x_1^{(m)}(t) + x_2^{(m)}(t), \tag{19}$$

where

$$x_1^{(m)}(t) = \sum_{J=1}^{l} \sum_{k=-\infty}^{k=\infty} \begin{pmatrix} e^{irt} e^{(r'+\alpha_k d')t} \\ -ie^{-irt} e^{(r'+\alpha_k d')t} \end{pmatrix} \times \left\{ \begin{array}{c} \hat{T}(ik)[\hat{T}_A^*(ik) - \hat{T}^*(ik)] \sum_{n=p_J+1}^{p_{J=1}} e^{ika_0(m+n)} e^{ik_o a_0 n} - \\ \hat{T}(ik)\hat{T}_B^*(ik) \sum_{n=p_J+1}^{p_{J=1}} e^{ika_0(m-n)} e^{ik_o a_0 n} \end{array} \right\} \tag{20}$$

and

$$x_2^{(m)}(t) = |\hat{T}(ik_0)|^2 \begin{pmatrix} e^{i(rt+k_0 a_0 m)} e^{(r'+\alpha_{k_0} d')t} \\ -ie^{i(-rt+k_0 a_0 m)} e^{(r'+\alpha_{k_0} d')t} \end{pmatrix}. \tag{21}$$

The functions, $\hat{T}(ik)$, $\hat{T}_A(ik)$, and $\hat{T}_B(ik)$ contain the structural information about the architecture of the network (i.e., number, length and position of the side chains). Information concerning the architecture of the multicellular network is therefore embedded into the composition excursion, $x^{(m)}(t)$. It is therefore possible that a cell at some location $m > p_l$ undergoes composition fluctuations that are representative of the spatial organization of the cells in the entire network. To understand in more details the relationship between the composition excursions and the architecture, we focus on the analysis of the second term in Eq. (19), that is, Eq. (21). This is the simplest term contributing to the composition excursions that can be analyzed. However, the first term [Eq. (20)] contains structural information similar to that of Eq. (21) but in a less transparent form. Equation (21) can be visualized as a traveling wave with amplitude decaying spatially. The prefactor $|\hat{T}(ik_0)|^2$ has all the properties of a transmission coefficient. This transmission coefficient along the backbone of the network is defined as $u(D)/U(D)$ and can be calculated numerically using Eq. (18b) for systems containing more that one side branch. In the analytical case of a single side-branch, for $0 \leq ka_0 < \pi$, there are exactly $L'$ transmission zeros at which $|\hat{T}(ik)|^2 \approx 0$. These zeros are located at $z_{ka_0}^{(\nu)} = (\pi/2)(2\nu+1)/(2L'+1)$ for $\nu = 0, 1, \ldots, L'$. This result reveals a quasistanding wave nature to the left of the side branch ($m \leq 0$). The first part in each row of Eq. (13) represents a proper standing wave weighted by $\hat{T}(ik)^*$. The second term in both rows represent traveling waves weighted by $|\hat{T}(ik_0)|^2$. At the transmission zeros of $|\hat{T}(ik_0)|^2$, the traveling-wave components are cancelled, leaving behind a proper standing wave pattern for each reactant weighted by $\hat{T}(ik)^*$, a nonzero complex number in general. The properties of the transmission coefficient are described in more details in Sec. III for networks composed of multiple side branches of various lengths as well as positions along the backbone.

## III. RESULTS AND DISCUSSION

In this section we report signal transmission spectra for several contrived network models that exhibit different structural features. We pay particular attention to specific signatures of the architecture in the form of pass and stop bands in the transmission spectra. We consider networks composed of side branches of lengths ranging from 1 to 5 cells and separation distances between adjacent side branches ranging from 1 to 4 intercellular spacings. These numbers are based on experimental and theoretical observations of vascular network formation *in vitro* [20,21]. In these studies, the authors found that the chord length in the percolation network of endothelial cells that form during the early stages of assembly of vascular networks on two-dimensional (2D) gels range between approximately 100–200 $\mu$m. This interval corresponds to a range of 3–6 cells if one considers that endothelial cells possess an average length of approximately 30 $\mu$m.

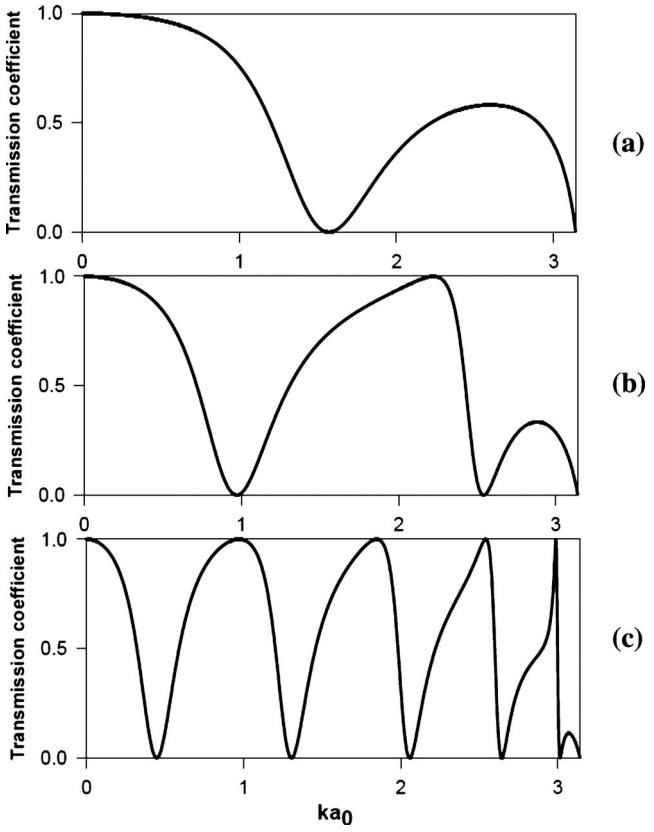


FIG. 2. Transmission coefficient $|\hat{T}(ik_0)|^2$ along the infinite multicellular chain backbone as a function of $ka_0$ for three lengths, $L'$, of a single side branch: (a) $L'=1$, (b) $L'=2$, and (c) $L'=5$.

We first consider the model of a single finite-length side branch grafted on an infinite backbone. The transmission spectra of Fig. 2 illustrate the effect of the number of endothelial cells in the side chain. These spectra exhibit zeros of transmissions at specific wave numbers (see Sec. II for exact analytical expression for $z_{ka_0}$). The transmission drops to zero at $ka_0 = \pi$ and beyond as the eigenvectors become nonpropagative. The zeros of transmission are associated with a resonant coupling between the oscillatory modes of the backbone and of the side chain. There is a one-to-one relation between the number of zeros of transmission and the number of cells in the side chain. It is therefore possible for a cell located in the backbone some distance away from the side branch to sense its presence as well as the number of cells that constitute it. This sensing may take place in the form of frequency dependent calcium sensing mechanisms. For in-

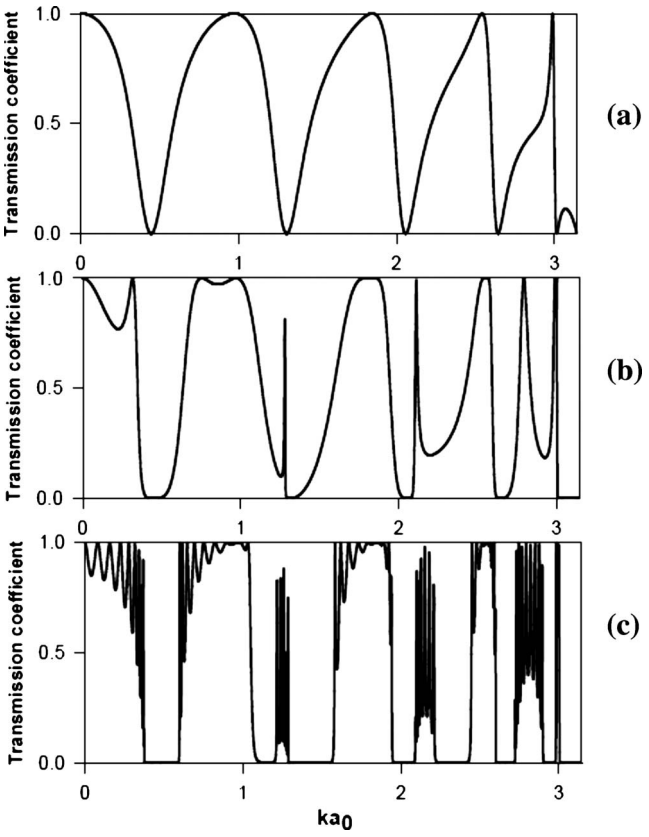


FIG. 3. Transmission coefficient, $|\hat{T}(ik_0)|^2$ along the infinite multicellular chain backbone as a function of $ka_0$ for (a) $N_c=1$ side chain, (b) $N_c=2$ side chains at $p_1=0$ and $p_2=4$ and (c) $N_c=10$ side chains grafted periodically on backbone cells, 0, 4, 8, 12, etc. The length of the side chains is constant at $L'=5$.

stance it is known that calmodulin-dependent protein kinase II (CAM kinase II) is able to decode the frequency of $Ca^{2+}$ spikes into different amounts of the enzyme activity via autophosphorylation [22]. CaM kinase II associates with $Ca^{2+}$ bound calmodulin allowing autophosphorylation. CaM kinase II activity increases exponentially with $Ca^{2+}$ frequency. At high frequency the kinase does not have time to deactive between spikes leading to increase in activity. At low frequency the dissociation of calmodulin can take place between spikes thus rendering CaM kinase II inactive. CaM kinase II can be found in many different tissue and more specifically endothelial cells [23,24]. This type of frequency responsive intracellular mechanism offers a possible mechanism for endothelial cells to decode transmitted signals that encode multicellular architectural information such as those described in the present paper.

We now consider several side branches constituted of the same number of cells and arranged along the backbone with a constant spacing. Coupling of the resonant modes of each individual chain through the backbone leads to a broadening of the zeros of transmission due to degeneracy lifting. Figure 3(b) clearly shows the separation of the zeros of transmission into two transmission dips. One type of dip is associated with the original chain resonance and still exhibits complete absence of transmission. The second type of dip shows a finite transmission for a small number of side chains [2 side chains in Fig. 2(b)]. Upon an increase in the number of equally spaced side chains grafted to the backbone, the resonant dip widens into a stop band (i.e., band gap) for compositional waves. This widening suggests the possibility of reinforcement in the long-range order of the network through signal conduction. The transmission coefficient associated with the second type of dip reaches values approaching zero as the number of chains increases. For large numbers of side chains, the second-type dips form passing gaps in the transmission spectrum. These latter band gaps result from the scattering of compositional waves traveling along the backbone by a periodic array of side chains. The transmission spectrum of a cellular network composed of equally spaced side chains containing the same number of cells has therefore two signatures in the form of stop bands. One signature results from the resonant filtering of the side chains and depends on the number of cells in the side chains. The second spectral signature is associated with the periodic arrangement of the side chains along the backbone.

The existence of spectral signatures in the form of zeros of transmission and stop bands that are characteristic of two different structural features of the network would therefore allow cells along the backbone to sense the architecture of the network via, as discussed earlier, $Ca^{2+}$ signal frequency-dependent phosphorylation. A question that arises is the separability of these signatures. To answer this question, we report in Fig. 4 the effect of random variations in the length of the side chains and the separation distance between the chains on the transmission spectrum of compositional waves along the backbone. The transmission spectra in Figs. 4(a) and 4(b) are obtained by generating the positions $p$ and/or lengths $L'$ of the side chains from a uniform distribution of random numbers within desired lower and upper limits. Figure 4(c) is the reference spectrum where all chains have the same length (side chain composed of five cells) and same separation distance (four backbone cell spacing). Randomization of the separation distance between the side chains eliminates some of the passing bands [see Fig. 4(b)] that were present in the reference spectrum but retains passing bands centered on $ka_0$ equal to 0.9, 1.85, 2.5, and 3. Considering a periodically grafted side chains with random length, the spectrum of Fig. 4(a) still possesses a set of passing bands centered on $ka_0$ of 1.2, 2.2, 2.9. While the low wavenumber passing band is retained in both cases of random structures, the other passing bands observed for the random spacing or the random length structures belong to two different separable sets. These two separate sets of passing bands are both present in the periodic constant length network. Finally, we calculated the transmission spectrum for a structure with simultaneous randomness in chain spacing and chain length (not illustrated). In this case only the small wavenumber passing band survives with zero transmission for all other wave numbers. The separability on the scale of wave numbers of the passing bands associated with the side chains length and separation distance indicate that cells along the backbone distance away from the side chains might be able to distinguish the structural features of the network architecture. This separability results from the fact that the stop bands in transmission along the main chain have two different origins, one originates from resonances with the

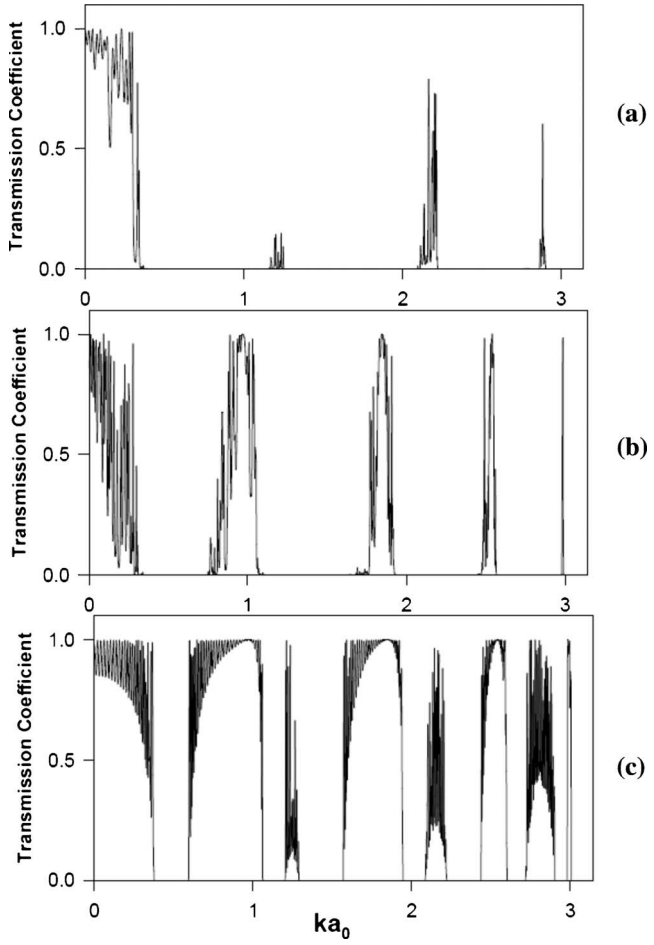


FIG. 4. Transmission coefficient, $|\hat{T}(ik_0)|^2$ along the infinite multicellular chain backbone as a function of $ka_0$ for (a) $N_c=100$ side chains with fixed spacing $p_{i+1}-p_i=4$ and length, $L'$, distributed randomly between 1 and 5, (b) $N_c=100$ side chains with fixed length $L'=5$ but with chain spacing $p_{i+1}-p_i$ randomly distributed between 1 and 4, and (c) $N_c=40$ side chains arranged periodically every four cells and with fixed length $L'=5$.

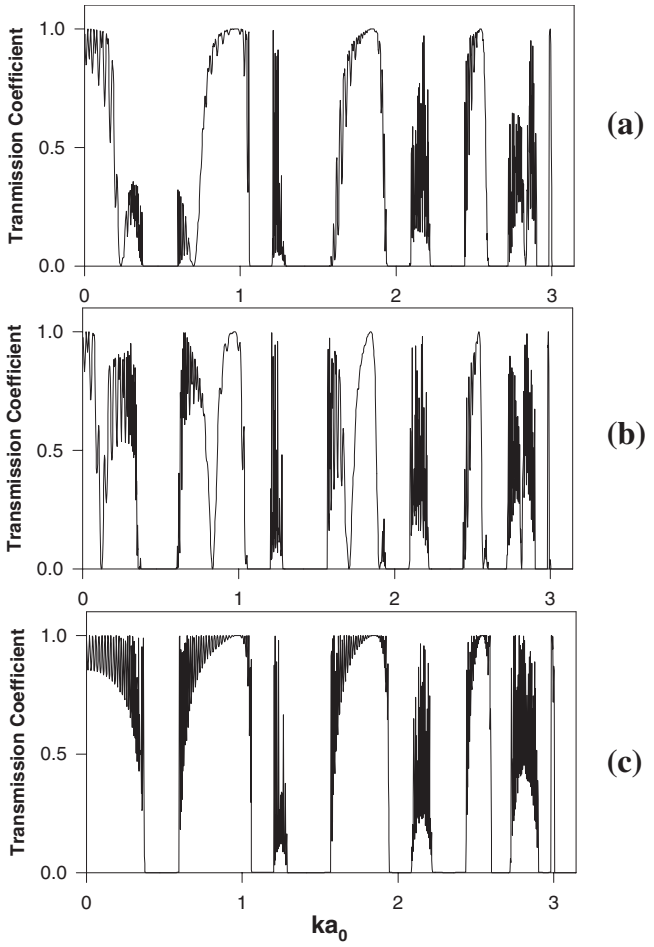


FIG. 5. Transmission coefficient, $|\hat{T}(ik_0)|^2$ along the infinite multicellular chain backbone as a function of $ka_0$ for $N_c=40$ side chains with fixed spacing $p_{i+1}-p_i=4$ and fixed length, $L'=5$ but for chain 20 which has a length of (a) 10 cells and (b) 20 cells. (d) is the reference network with the 20th chain five-cell long.

side branches that are nearly position independent but length dependent and a second one results from scattering by the periodic arrangement of the side branches.

Finally, we illustrate in Fig. 5, the separation of structural information in the transmission spectrum of a periodic array of equal length side chains with one single defect. This defect takes the form of a single chain with an unusually long length. Two lengths of the defect chain are considered (10 and 20 cells). The overall spectrum of the defected architectures retains the characteristics of the perfect reference one. However, one clearly identifies zeros of transmission that form within the passing bands of the reference system. The number of zeros of transmission and the wave number at which they occur depends on the number of cells within the defected chain. The wave number of the narrow defect stop bands [Figs. 5(a) and 5(b)] might, therefore, enable a backbone cell to sense the presence of the defect. The position of the defect chain in the periodic array of side chains does not produce a specific signature (not shown).

## IV. CONCLUSIONS

We present a theoretical model for information transfer in complex cellular networks representative of endothelial cells in the vascular tree. This model enables the calculation of the transmission spectrum of propagating compositional waves in multicellular architectures. We consider compositional waves originating from negative feedback loops between $Ca^{2+}$ and $IP_3$ in endothelial cells, an important signaling system in endothelial cells. These waves are shaped by the connection topologies of the networks of endothelial cells. A model of linear endothelial cell chain with side branches reveals two mechanisms that control global signal propagation, namely, resonance filtering and scattering by periodic structures. It is seen that both the length and position of side branches affect the long-range compositional wave behavior, i.e., the ability of the network to "communicate" information regarding long-range order. This information is encoded in a transmission spectrum of compositional waves which necessitates cellular control over calcium and $IP_3$ self-regulation as well as oscillation frequency via calcium regulation of $IP_3$ concentration. The structural information encoded in the

wave-number (frequency) transmission spectrum might, therefore, be decodable by individual cells, for instance, via intracellular pathways such as frequency-dependent protein phosphorylation by a $Ca^{2+}$-calmodulin activated kinase [22].

The objective of this paper is to demonstrate the existence of architecture-dependent signals in multicellular networks. It is hoped that our model can provide a framework for designing new experiments to identify similar signal mechanisms in biological media constituted of endothelial cell networks. Examples of such networks include mature or immature vasculatures. We focused in the present paper on networks composed of finite side branches attached to a backbone as prototypical models of complex architectures. While these networks may be a reasonable representation of an immature plexus, they do not represent the hierarchical vascular tree of a mature vasculature. The Green's-function-based method we have used here, however, is able to handle network architectures composed of loops and segments of endothelial cells organized in parallel and series arrangements as more realistic descriptions of mature vascular networks. Finally, the linear method that we reported, likely needs to be extended to include nonlinear effects to account for signal conduction beyond small excursion from stable compositional points.


[1] E. A. V. Jones, F. le Noble, and A. Eichmann, Physiology **21**, 388 (2006).

[2] S. S. Nunes, K. A. Greer, C. M. Stiening, H. Y. Chen, K. R. Kidd, M. A. Schwartz, C. J. Sullivan, H. Rekapally, and J. B. Hoying, Microvasc. Res. **79**, 10 (2010).

[3] T. W. Secomb and A. R. Pries, Microcirculation (Philadelphia) **9**, 377 (2002).

[4] A. R. Pries and T. W. Secomb, Microcirculation (Philadelphia) **15**, 753 (2010).

[5] S. S. Segal, D. G. Welsh, and D. T. Kurjiaka, J. Physiol. **516**, 283 (1999).

[6] Y. N. Tallini, J. F. Brekke, B. Shui, R. Doran, S. Hwang, J. Nakai, G. Salama, S. S. Segal, and M. I. Kotlikoff, Circ. Res. **101**, 1300 (2007).

[7] K. A. Dora, Semin Cell Dev. Biol. **12**, 27 (2001).

[8] T. Fauquier, N. C. Guérineau, R. A. McKinney, K. Bauer, and P. Mollard, Proc. Natl. Acad. Sci. U.S.A. **98**, 8891 (2001).

[9] *Interdisciplinary Applied Mathematics*, edited by C. P. Fall, E. S. Marland, J. M. Wagner, and J. J. Tyson (Springer, New York, 2000), Vol. 20.

[10] M. Eray, P. A. Deymier, J. H. Hoying, K. Runge, and J. O. Vasseur, Physica D **237**, 2777 (2008).

[11] H. G. Othmer and L. E. Scriven, Ind. Eng. Chem. Fundam. **8**, 302 (1969).

[12] H. G. Othmer and L. E. Scriven, J. Theor. Biol. **32**, 507 (1971).

[13] A. Politi, L. D. Gaspers, A. P. Thomas, and T. Hofer, Biophys. J. **90**, 3120 (2006).

[14] R. Thomas and M. Kaufman, Chaos **11**, 170 (2001).

[15] L. Dobrzynski, Surf. Sci. Rep. **6**, 119 (1986).

[16] J. O. Vasseur, A. Akjouj, L. Dobrzynski, B. Djafari-Rouhani, and E. H. El Boudouti, Surf. Sci. Rep. **54**, 1 (2004).

[17] L. Dobrzynski and H. Puszkarski, J. Phys.: Condens. Matter **1**, 1239 (1989).

[18] B. Sylla, L. Dobrzynski, and H. Puszkarski, J. Phys.: Condens. Matter **1**, 1247 (1989).

[19] A. Akjouj, B. Sylla, and L. Dobrzynski, Ann. Phys. (Paris) **18**, 363 (1993).

[20] A. Gamba, D. Ambrosi, A. Coniglio, A. de Candia, S. Di Talia, E. Giraudo, G. Serini, L. Preziosi, and F. Bussolino, Phys. Rev. Lett. **90**, 118101 (2003).

[21] G. Serini, D. Ambrosi, E. Giraudo, A. Gamba, L. Preziosi, and F. Bussolino, EMBO J. **22**, 1771 (2003).

[22] P. De Koninck and H. Schulman, Science **279**, 227 (1998).

[23] Z. Balla, B. Hoch, P. Karczewski, and I. E. Blasig, J. Biol. Chem. **277**, 21306 (2002).

[24] H. Cai, D. Liu, and J. G. N. Garcia, Cardiovasc. Res. **77**, 30 (2008).